

Title no. 98-S76

# Proposed Design of High-Strength Spiral Reinforcement in Compression Members

by Stephen Pessiki, Benjamin Graybeal, and Michael Mudlock

*Current provisions of the ACI 318 Code and AASHTO Design Specification limit the nominal yield stress of spiral reinforcement for compression members to 414 MPa (60 ksi). A procedure for the design of high-strength spiral reinforcement for compression members is proposed and evaluated. The proposed method utilizes usable stress values, rather than nominal yield stress values, for spiral design. The research included large-scale axial load tests on 14 spirally reinforced concrete compression members with spiral reinforcement yield stress values ranging from 538 to 1345 MPa (78 to 195 ksi) and usable stress values ranging from 545 to 1131 MPa (79 to 164 ksi). It was found that, for the compression member geometries and material properties treated in this study, the proposed design procedure satisfactorily predicted the behavior of the compression members made from spirals with usable stress values up to 758 MPa (110 ksi).*

**Keywords:** concrete; high-strength steel; reinforcement.

## INTRODUCTION

In current U.S. practice, spiral reinforcement in compression members is designed so that, should the compression member be overloaded, the spiral reinforcement provides enough strength enhancement to the concrete core to replace the strength lost by the spalling of the concrete cover. For a given compression member cross section, a higher-strength concrete requires a greater volume of spiral reinforcement. As concrete strengths have increased over the years, the required amount of spiral reinforcement has also increased. To satisfy the need for a greater amount of spiral reinforcement, either the use of larger diameter spiral wires or decreased pitch can be employed. Fabrication problems and concrete placement difficulty based on practical spacing limits and code requirements may result, however.

One alternative to the aforementioned practices is to use higher-strength spiral reinforcement, wherein a smaller amount of higher-strength spiral steel is used to provide a given required amount of confining pressure to the concrete. Current provisions of the ACI 318 Building Code Requirements for Structural Concrete<sup>1</sup> (hereafter referred to as the ACI 318 Code) and the American Association of State Highway and Transportation Officials LRFD Bridge Design Specifications<sup>2</sup> (hereafter referred to as the AASHTO Design Specification), however, limit the spiral reinforcement yield stress to 414 MPa (60 ksi).

This paper is comprised of three parts. The first part describes an initial series of tests that were performed (Series 1) to evaluate the confinement effectiveness of high-strength spiral reinforcement in compression members. Based on the results of these tests, a procedure for the design of high-strength spiral reinforcement was developed. This design procedure is presented in the second part of the paper. Finally, the third part of the paper describes additional tests that were

performed (Series 2) to evaluate the proposed design procedure. Complete details of the research presented in this paper are given in Graybeal<sup>3</sup>, Graybeal and Pessiki<sup>4</sup>, and Mudlock and Pessiki.<sup>5,6</sup>

## RESEARCH SIGNIFICANCE

A procedure for the design of high-strength spiral reinforcement for compression members is proposed and evaluated. It is shown that spiral reinforcement stresses in excess of 414 MPa (60 ksi) may be safely used in the design of concrete compression members. Use of spiral steel stresses in excess of 414 MPa (60 ksi) reduces the required volume of spiral reinforcement, and therefore reduces the construction problems associated with heavily reinforced members.

## BACKGROUND

In the early 1900s, Considère<sup>7</sup> found that the compressive strength of concrete was increased by transverse confining pressure. This confining pressure, whether active (that is, applied externally by a pressurized fluid) or passive (that is, created by lateral expansion of the axially compressed concrete against a confining material), worked to resist the lateral expansion of concrete as it was loaded axially. Richart, Brandzaeg, and Brown<sup>8,9</sup> and Richart and Brown<sup>10</sup> presented an equation of the following form to describe the relationship between the unconfined concrete strength  $f_{co}$ , lateral pressure  $f_{2-2}$ , and the confined concrete strength  $f_{c2}$

$$f_{c2} = f_{co} + 4.1f_{2-2} \quad (1)$$

Richart, Brandzaeg, and Brown also proposed the following equation that relates the longitudinal strain at the confined concrete strength  $\epsilon_{c2}$  to the confined strength  $f_{c2}$ , the unconfined strength  $f_{co}$ , and the corresponding unconfined longitudinal strain  $\epsilon_{co}$

$$\epsilon_{c2} = \epsilon_{co} \left( 5 \frac{f_{c2}}{f_{co}} - 4 \right) \quad (2)$$

Equations (1) and (2) are used as part of the proposed design procedure.

*ACI Structural Journal*, V. 98, No. 6, November-December 2001.

MS No. 00-168 received July 24, 2000, and reviewed under Institute publication policies. Copyright © 2001, American Concrete Institute. All rights reserved, including the making of copies unless permission is obtained from the copyright proprietors. Pertinent discussion will be published in the September-October 2002 *ACI Structural Journal* if received by May 1, 2002.

ACI Member **Stephen Pessiki** is an associate professor in the Department of Civil and Environmental Engineering at Lehigh University, Bethlehem, Pa. He is chairman of ACI Committee 228, Nondestructive Testing of Concrete. His research interests include the behavior and design of reinforced and prestressed concrete structures and the nondestructive evaluation of structures.

**Benjamin Graybeal** is a research engineer employed by PSI, Inc., working for the Federal Highway Administration's High Performance Materials Team at the Turner-Fairbank Highway Research Center. He received his BS and MS from Lehigh University, and is pursuing his doctorate at the University of Maryland. His research interests include large-scale structural testing of bridge components and nondestructive evaluation of highway structures.

**Michael Mudlock** is an engineer with Simpson, Gumpertz & Heger Inc. He received his BS and MS in civil engineering from Lehigh University.

### Idealized axial load behavior

Figure 1 shows the idealized axial load-axial shortening behavior of a spirally reinforced concrete compression member. Key loads  $P_1$ ,  $P_2$ , and  $P_{failure}$  indicate the loads at the initiation of cover loss, the confined peak, and the failure of the member (defined by fracture of the spiral reinforcement), respectively. Similarly,  $\Delta_1$ ,  $\Delta_2$ , and  $\Delta_{failure}$  indicate the axial shortening values at the corresponding loads. A concrete compression member without spiral reinforcement exhibits a load capacity approximately equal to  $P_1$  and a decrease in resistance with an increase in applied deformation beyond that point. Figure 1 shows that the presence of spiral reinforcement leads to a second peak in the response, and that this second peak is reached at a much greater ductility than is achieved by an unconfined member.

### Current design requirements

The ACI 318 Code and the AASHTO Design Specification both state that the nominal concentric axial load capacity  $P_o$  of a reinforced concrete compression member is given by

$$P_o = 0.85f_{co}(A_g - A_{st}) + A_{st}f_y \quad (3)$$

where  $A_g$  is the gross cross-sectional area of the compression member,  $A_{st}$  is the area of the longitudinal reinforcement, and  $f_y$  is the yield stress of the longitudinal reinforcement.

The volumetric ratio of spiral reinforcement in a compression member  $\rho_{sp}$ , defined as the ratio of the volume of the spiral to the volume of the concrete core, is computed as

$$\rho_{sp} = \frac{4A_{sp}}{d_{sp}s} \quad (4)$$

where the spiral wire cross-sectional area, pitch, and out-to-out diameter are  $A_{sp}$ ,  $s$ , and  $d_{sp}$ , respectively. The confining pressure  $f_{2-2}$  that is applied to the concrete core by spiral reinforcement is calculated as

$$f_{2-2} = \frac{1}{2}\rho_{sp}f_{sp} \quad (5)$$

where  $f_{sp}$  is the stress in the spiral reinforcement.

Spiral reinforcement is designed according to the philosophy that the strength reduction caused by spalling of the concrete cover should equal the strength gain of the concrete core due to confinement. In equation form, this is written as

$$0.85f_{co}(A_g - A_{core}) = 4.1f_{2-2}A_{core} \quad (6)$$

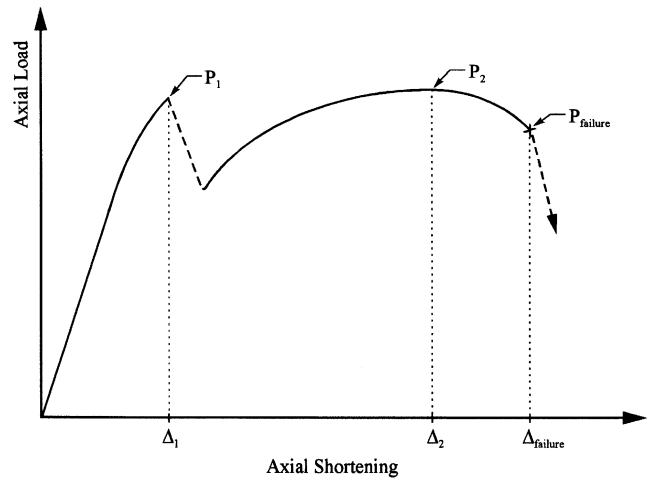


Fig. 1—Idealized axial load-axial shortening behavior of spirally reinforced concrete compression member.

where  $A_{core}$  is the area of the concrete core. Substituting Eq. (5) and solving for  $\rho_{sp}$  leads to

$$\rho_{sp} = 0.42 \frac{f_{co}}{f_{sp}} \left( \frac{A_g}{A_{core}} - 1 \right) \quad (7)$$

In the design codes, the 0.42 factor is increased slightly to 0.45, and the required amount of spiral reinforcement is given as

$$\rho_{sp} \geq 0.45 \frac{f_{co}}{f_{sy}} \left( \frac{A_g}{A_{core}} - 1 \right) \quad (8)$$

In Eq. (8), the stress in the spiral reinforcement  $f_{sp}$  is assumed to equal  $f_{sy}$ , the yield stress of the spiral reinforcement. Compression members designed using Eq. (8) are expected to exhibit the idealized behavior shown in Fig. 1.

### SERIES 1 TESTS

Table 1 describes the Series 1 tests. Also included in this table are the Series 2 tests that are described later. All specimens were loaded to failure in concentric axial compression. The primary variables treated in the eight Series 1 tests were specimen diameter  $d_c$  and spiral nominal yield stress  $f_{sy,nom}$ . Table 1 includes an alpha-numeric identifier for each specimen. The prefixes 24 and 14 refer to specimens with 610 and 356 mm (24 and 14 in.) diameters, respectively, and A, B, C, and D denote the spiral steel nominal yield stresses as follows: A = 538 MPa (78 ksi); B = 738 MPa (107 ksi); C = 834 MPa (121 ksi); and D = 965 MPa (140 ksi), respectively. These nominal yield stress values were provided by the spiral manufacturer.

### Specimen details

Table 1 also summarizes the details of each specimen. The 610 mm (24 in.) diameter specimens all measured 2.44 m (96 in.) in height, and the 356 mm (14 in.) diameter specimens all measured 1.42 m (56 in.) in height. Thus, all specimens had a height-diameter aspect ratio of 4-to-1. All specimens had a 51 mm (2 in.) concrete cover to the outside

of the spiral reinforcement. The design concrete compressive strength was 55.2 MPa (8.0 ksi).

Extra spiral reinforcement was provided in each specimen over one diameter of height from each end. The test region was the portion of the specimen between the more heavily confined end regions. Within each test region, the spiral reinforcement was designed according to the ACI 318 Code based on the design concrete compressive strength and the manufacturer-supplied nominal yield stresses. The Code limit of 414 MPa (60 ksi) was ignored. All spiral wires treated in the Series 1 tests had a diameter  $d_{sw}$  of 8.9 mm (0.35 in.). Two wires were bundled to create the spiral in Specimens 14-A, 14-B, 24-A, and 24-B. This is shown in Table 1, where  $n_{sp}$  is the number of wires in the bundle. Mild steel longitudinal reinforcement held the spiral in position during fabrication.

### Instrumentation

Twelve electrical resistance strain gages were used to monitor strains in both the spiral and longitudinal reinforcement within the test region, and linear variable differential transformer displacement transducers (LVDTs) were used to measure overall axial shortening.

### Concrete properties

The unconfined concrete compressive strength was determined from tests of 152 x 305 mm (6 x 12 in.) field-cured cylinders and cores. The unconfined concrete compressive strength was also computed from the first peak  $P_1$  in the axial load response of each specimen. Based on the results of the compression tests, the unconfined concrete compressive strength  $f_{co}$  was 58.6 MPa (8.5 ksi), and the corresponding axial strain  $\epsilon_{co}$  was 0.0027.

### Steel properties

According to the spiral manufacturer, the spiral reinforcement treated in the study was produced through a cold-drawing process from four different grades of undeformed steel wire. Each steel wire was then turned in to a spiral such that the outer spiral diameter was 508 and 254 mm (20 and 10 in.), respectively, for the 610 and 356 mm (24 and 14 in.) diameter specimens. No stress-relieving was performed either before or after the wire was turned into a spiral. The spiral manufacturer performed material testing on the spiral wire after the drawing process, but before the wire had been turned into a spiral.

Tension tests were performed on lengths of spiral wire that were cut from the 508 mm (20 in.) diameter spirals for all four grades of steel. The wires were first straightened as much as possible by bending prior to the tension tests. Strain gages were placed along the longitudinal axis of the wire to obtain axial strain readings.

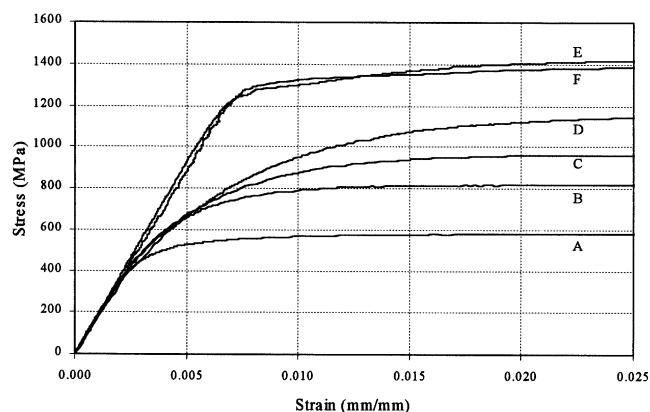
Turning a steel wire into a spiral causes permanent plastic deformations and residual stresses within the cross section of the wire and thus changes the mechanical properties of the wire. Therefore, a spiraled length of wire will not exhibit the same tensile stress-strain properties as a similar length of wire that was never spiraled. Straightening a spiraled wire further changes the residual stresses within the cross section, and thus further changes the tension stress-strain properties of the wire. References 3 and 4 explain in detail the effects of spiraling on the stress-strain properties of spiral wire.

Figure 2 shows the tensile stress-strain curves that were obtained from the sections of spiraled-straightened wire. Included in the figure are results from the wires used in

**Table 1—Description of test specimens**

Specimen Identification	Spiral reinforcement								Longitudinal reinforcement	
	$d_c$ , mm	$f_{sy, nom}$ , MPa	$f_{sp2, dsgn}$ , MPa	$d_{sw}$ , mm	$n_{sp}$	$A_{sp}$ , mm <sup>2</sup>	$s$ , mm	$\rho_{sp}$ , %	Bars	$\rho_l$ , %
Series 1										
24-A	610	538	—	8.9	2	124	48	2.05	6-No. 4	0.26
24-B	610	738	—	8.9	2	124	64	1.54	6-No. 4	0.26
24-C	610	834	—	8.9	1	62	38	1.28	6-No. 4	0.26
24-D	610	965	—	8.9	1	62	44	1.10	6-No. 4	0.26
14-A	356	538	—	8.9	2	124	44	4.40	4-No. 4	0.51
14-B	356	738	—	8.9	2	124	60	3.24	4-No. 4	0.51
14-C	356	834	—	8.9	1	62	35	2.80	4-No. 4	0.51
14-D	356	965	—	8.9	1	62	38	2.57	4-No. 4	0.51
Series 2										
14-A'	356	538	545	8.9	2	124	41	4.76	4-No. 4	0.51
14-B'	356	738	717	8.9	2	124	54	3.62	4-No. 4	0.51
14-C'	356	834	745	8.9	1	62	28	3.48	4-No. 4	0.51
14-D'	356	965	758	8.9	1	62	29	3.42	4-No. 4	0.51
14-E'	356	1345	1131	9.1	1	65	44	2.29	4-No. 4	0.51
14-F'	356	1276	1110	10.9	1	93	62	2.34	4-No. 4	0.51

Note: 1 ksi = 6.985 MPa, and 1 in. = 25.4 mm.



*Fig. 2—Stress-strain behavior of spiral wire tested at Lehigh University.*

the Series 2 tests, which are discussed in a following section. Results are plotted up to a strain of 0.025. Table 2 summarizes the results of the tension tests both as reported by the spiral manufacturer and as determined from the tension testing performed at Lehigh University. The spiral manufacturer used an elongation under load method, as described in ASTM A 370. This standard is referenced from ASTM A 82, which defines standards for steel wire used as concrete reinforcement. The elongation under load method is generally used for determining the tensile yield properties of a steel tensile specimen that does not

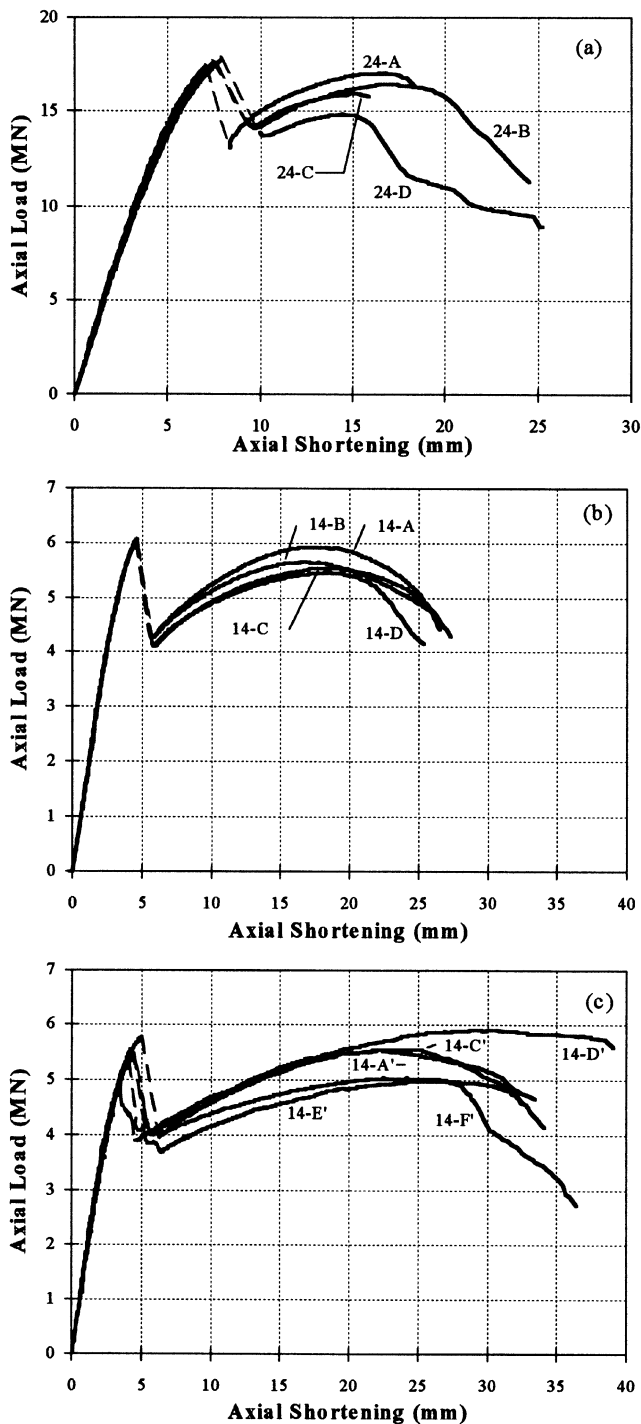


Fig. 3—Axial load-axial shortening responses: (a) Series 1, 610 mm (24 in.) diameter specimens; (b) Series 1, 356 mm (14 in.) diameter specimens; and (c) Series 2, 356 mm (14 in.) diameter specimens.

exhibit a well-defined yield point. In the Lehigh University tests, the 0.2% offset method was used to define yield.

Table 2 shows that the yield stresses determined from the spiraled-straightened steel tests performed at Lehigh University are below the yield stresses determined by the spiral manufacturer. This is attributed to both the effects of spiraling and straightening on the wire as well as the different methods used to determine yield. Finally, equations were fit to the curves shown in Fig. 2. Details are given in References

Table 2—Spiral reinforcement properties

Spiral wire	Manufacturer reported yield stress, MPa	Lehigh 0.2% offset yield stress, MPa
A	538 (unspiraled)	524 (straightened)
B	738 (unspiraled)	703 (straightened)
C	834 (unspiraled)	752 (straightened)
D	965 (unspiraled)	765 (straightened)
E	1345 (unspiraled)	1296 (unspiraled)
F	1276 (unspiraled)	1331 (unspiraled)

Note: 1 ksi = 6.895 MPa.

3 and 4. These equations are used to obtain spiral stresses from the spiral strains measured during the tests.

### Loading procedure

Each 610 mm (24 in.) diameter specimen was tested under concentric axial compression in a 22.2 MN (5000 kip) capacity universal testing machine. Through the initial portion of the test, the load rate was approximately 311 kN/min (70 kips/min), which corresponded to a stress rate of about 1069 kPa/min (155 psi/min) and an axial shortening rate of approximately 0.102 mm/min (0.0040 in./min). Once the desired load rate was achieved during the initial linear portion of the load-shortening behavior, no further adjustments were made to the testing machine. As a result, the actual load rate applied to each specimen decreased as the specimen softened.

The 356 mm (14 in.) diameter specimens were tested in a similar manner as the 610 mm (24 in.) diameter specimens. Through the initial portion of the test, the load rate was about 107 kN/min (24 kips/min), which corresponded to a stress rate of about 1069 kPa/min (155 psi/min) and an axial shortening rate of approximately 0.058 mm/min (0.0023 in./min).

### Axial load behavior

The axial load-axial shortening responses of the Series 1 specimens are shown in Fig. 3(a) and (b). Table 3 presents key results obtained from the Series 1 tests. As shown in the figures, each specimen exhibited the expected axial load-axial shortening behavior illustrated in Fig. 1, with no noticeable decrease in ductility for the compression members made with the higher-strength spirals.

Failure of all eight specimens was defined by rupture of one or more turns of wire of the spiral reinforcement and a subsequent loss of confining pressure on the concrete core. This resulted in a significant decrease in the load-carrying capacity of the specimen. Two observations, however, indicate that the failures were not due to the spiral reinforcement reaching its ultimate strain as caused by lateral expansion of the core. First, for all specimens, the measured strain in the spiral reinforcement just before failure was less than one-third of the spiral strain at ultimate stress  $\epsilon_{su}$ . Typically, the maximum strains measured during the tests were less than 0.01. Second, for most of the specimens, multiple spiral fractures occurred simultaneously along a well-defined inclined plane throughout the test region. This suggests that the plane formed first, and that the spirals fractured as a result of relative movement of the concrete along this plane.

### Spiral behavior

Table 3 presents values for  $f_{sp2,exp}$ , which are single value approximations for the experimentally obtained range of stresses obtained in the spiral reinforcement at  $\Delta_2$ . The values of  $f_{sp2,exp}$  show that the higher yield stress specimens

**Table 3—Summary of results of Series 1 tests**

Series 1													
Design		Experiment						Richart, Brandzaeg, and Brown		Ratios			
Identification	$f_{sy,nom}$ , MPa	$\Delta f_{c12,dsgn}$ , MPa	$f_{sp2,exp}$ , MPa	$P_2$ , MN	$f_{c2,exp}$ , MPa	$\Delta f_{c12,exp}$ , MPa	$\epsilon_{c2,exp}$	$\Delta f_{c12,Rich}$ , MPa	$\epsilon_{c2,Rich}$	$R(f_{sp2})_{exp/f_{sy,nom}}$	$R(\Delta f_{c12})_{exp/dsgn}$	$R(\Delta f_{c12})_{exp/Rich}$	$R(\epsilon_{c2})_{exp/Rich}$
24-A	538	23.1	483	17.02	82.5	23.9	0.0088	20.7	0.0082	0.90	1.03	1.15	1.07
24-B	738	23.7	655	16.42	79.4	20.8	0.0081	21.0	0.0075	0.89	0.88	0.99	1.08
24-C	834	22.4	586	15.92	77.0	18.4	0.0076	15.7	0.0069	0.70	0.82	1.17	1.10
24-D	965	22.1	586	14.84	71.6	13.0	0.0093	13.4	0.0057	0.61	0.59	0.97	1.64
14-A	538	50.3	552	5.95	113.5	54.9	0.0113	51.5	0.0153	1.03	1.09	1.07	0.74
14-B	738	50.8	655	5.68	108.1	49.5	0.0159	45.1	0.0141	0.89	0.97	1.10	1.13
14-C	834	49.6	793	5.55	105.7	47.1	0.0183	45.1	0.0135	0.95	0.95	1.04	1.36
14-D	965	52.6	862	5.46	103.9	45.3	0.0194	47.0	0.0131	0.89	0.86	0.96	1.48

Note: 1 kip = 0.00445 MN; 1 ksi = 6.895 MPa; and 1 in. = 25.4 mm.

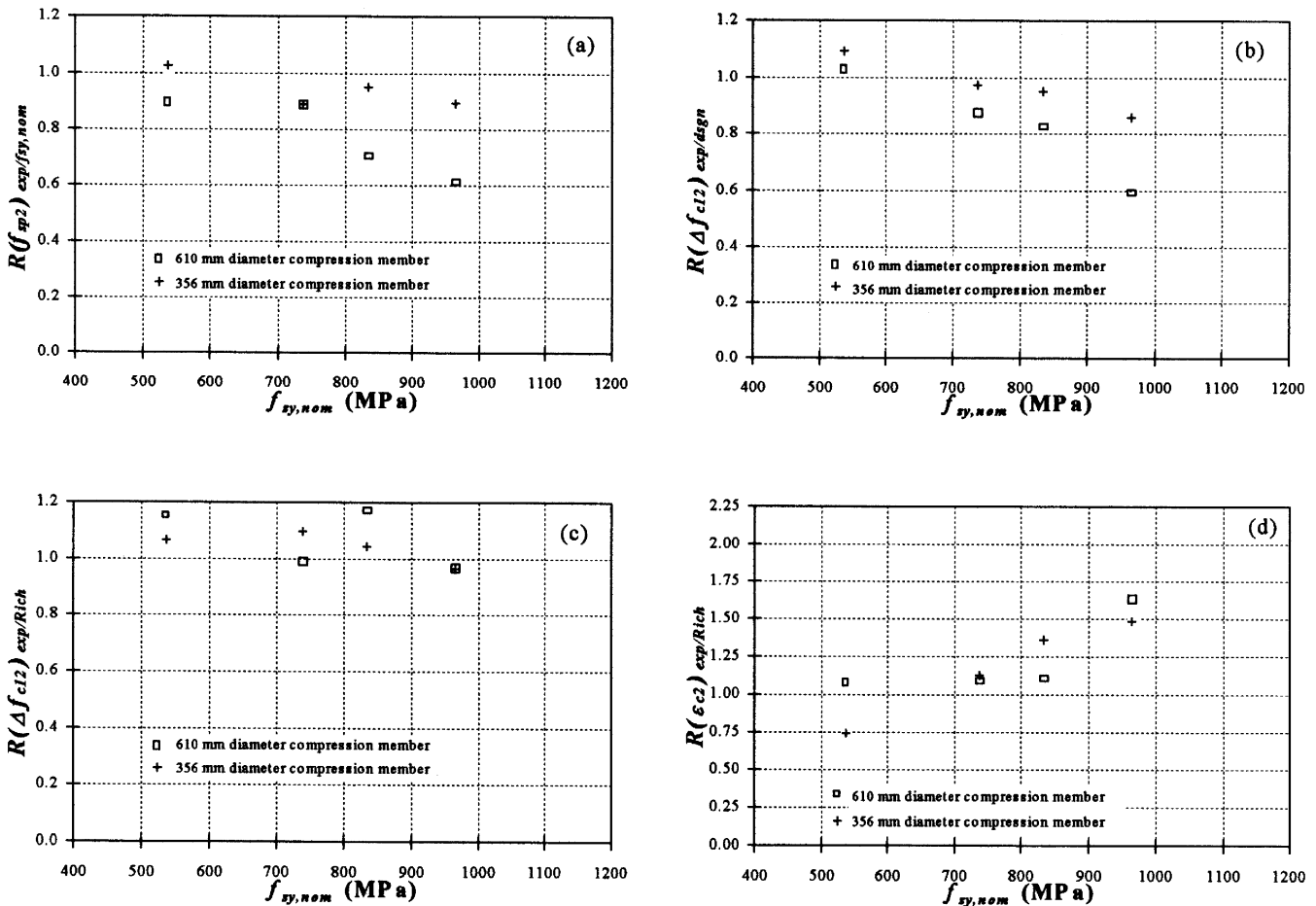


Fig. 4—Series 1 results: (a)  $R(f_{sp2})_{exp/f_{sy,nom}}$  versus  $f_{sy,nom}$ ; (b)  $R(Df_{c12})_{exp,dsgn}$  versus  $f_{sy,nom}$ ; (c)  $R(Df_{c12})_{exp,Rich}$  versus  $f_{sy,nom}$ ; and (d)  $R(\epsilon_{c2})_{exp,Rich}$  versus  $f_{sy,nom}$

did reach stresses in excess of 414 MPa (60 ksi), but not the design yield stress. Table 3 shows  $R(f_{sp2})_{exp/f_{sy,nom}}$ , the ratio of the spiral stress at  $\Delta_2$  to the nominal design value of the spiral yield stress. This ratio is also plotted in Fig. 4(a) versus the nominal spiral yield stress.  $R(f_{sp2})_{exp/f_{sy,nom}}$  ranges from 0.61 to 1.03, and in only one case, Specimen 14-A, was  $f_{sp2,exp}$  above  $f_{sy,nom}$ .

Two observations are made from Table 3 and Fig. 4(a). First, in general, the spirals in the smaller diameter specimens reached a greater fraction of the design yield stress as

compared with the spirals in the larger diameter specimens. Second, the stress in the spiral reinforcement was closer to the design yield stress in the lower nominal yield stress specimens. In the higher yield stress specimens, especially for the larger diameter specimens, the stress in the spiral was significantly below the nominal yield value.

**Confined concrete strength**

The axial stress in the concrete core at  $\Delta_2$  is denoted as  $f_{c2,exp}$ . To obtain this stress, the force carried by the longitudinal

reinforcement  $P_s$  was subtracted from the total force carried by the specimen  $P_2$ . The axial stress in the core was then determined by dividing the remaining force carried by the area of the core concrete  $A_{core}$ . This is expressed in equation form as

$$f_{c2,exp} = \frac{P_2 - P_s}{A_{core}} \quad (9)$$

Equation (9) assumes that the concrete cover carries no axial force after cover failure has occurred. This assumption is consistent with the visual observations made during the tests.

The experimentally determined increase in the strength of the confined concrete core  $\Delta f_{c12,exp}$  was computed as the stress in the confined core at the second peak  $f_{c2,exp}$  minus the unconfined compressive strength  $f_{co}$

$$\Delta f_{c12,exp} = f_{c2,exp} - f_{co} \quad (10)$$

In the following paragraphs, the experimentally determined increase in strength of the confined core is compared with the design increase in strength of the confined core  $\Delta f_{c12,dsgn}$  and also to the increase in strength of the confined core calculated from the experimentally determined stress in the spiral reinforcement and the confinement relationship proposed by Richart, Brandzaeg, and Brown,  $\Delta f_{c12,Rich}$ .

The design value of the increase in strength of the confined core  $\Delta f_{c12,dsgn}$  is calculated from Eq. (11), which is a combination of Eq. (1) and (5)

$$\Delta f_{c12,dsgn} = 2.05 \rho_{sp} f_{sy,nom} \quad (11)$$

Table 3 shows the experimental and design values for  $\Delta f_{c12}$  and  $R(\Delta f_{c12})_{exp/dsgn}$ , which is the ratio of  $\Delta f_{c12,exp}$  to  $\Delta f_{c12,dsgn}$ . In Fig. 4(b), this ratio is plotted versus the nominal spiral yield stress of each specimen. Table 3 and Fig. 4(b) show that six of the eight specimens did not achieve the level of strength enhancement that was expected based on the spiral design yield strength. For the 356 mm (14 in.) diameter specimens,  $R(\Delta f_{c12})_{exp/dsgn}$  ranged from 0.86 to 1.09, with Specimens 14-A, 14-B, and 14-C all achieving at least 95% of the design strength enhancement. For the 610 mm (24 in.) diameter specimens, the ratio ranged from 0.59 to 1.03, with only Specimen 24-A achieving at least 95% of the design strength enhancement. For both diameter specimens, the strength increase achieved was greater for the specimens with lower yield stress spirals than it was for the specimens with higher yield stress spirals.

The strength increase of the confined core  $\Delta f_{c12,Rich}$ , calculated from the experimentally obtained stress in the spiral reinforcement ( $f_{sp2,exp}$  in Table 3), is calculated from Eq. (12), which is a combination of Eq. (1) and (5)

$$\Delta f_{c12,Rich} = 2.05 \rho_{sp} f_{sp2,exp} \quad (12)$$

Table 3 shows the experimental and Richart, Brandzaeg, and Brown-predicted values of  $\Delta f_{c12}$  and  $R(\Delta f_{c12})_{exp/Rich}$ , which is the ratio of  $\Delta f_{c12,exp}$  to  $\Delta f_{c12,Rich}$ . In Fig. 4(c), this ratio is also plotted versus the nominal spiral yield stress of each specimen. These ratios, which range from 0.97 to 1.17, show that all eight specimens exhibited experimental strength increases consistent with the measured stresses in

the spiral reinforcement. Therefore, for the specimens treated in the Series 1 tests, Eq. (1) adequately represents the relationship between confining pressure and the strength enhancement of the core concrete. It is emphasized that the equation is accurate only if the actual confining pressure is used. The equation may not provide accurate results if a confining pressure is used which is based on the nominal yield stress of the spiral reinforcement.

### Longitudinal strains

An experimental value of longitudinal strain at  $\Delta_2$  was obtained from the strain measurements in the longitudinal steel reinforcement. This value,  $\epsilon_{c2,exp}$ , was calculated as the average strain measured in the longitudinal reinforcement at  $\Delta_2$ . Table 3 shows the value of  $\epsilon_{c2,exp}$  for each specimen.

As noted previously, Eq. (2) was proposed by Richart, Brandzaeg, and Brown to predict the axial strain at peak confined compressive strength. The applicability of Eq. (2) was examined by substituting into it the experimentally determined values for  $\epsilon_{co}$ ,  $f_{c2,exp}$ , and  $f_{co}$ . The axial strain computed by this equation is referred to as  $\epsilon_{c2,Rich}$ . The values of  $\epsilon_{co}$  and  $f_{co}$  were taken as 0.0027 and 8.50 ksi (58.6 MPa), respectively. The value of  $f_{c2,exp}$  was determined from Eq. (9).

Table 3 shows the experimentally obtained values and Richart, Brandzaeg, and Brown-predicted values of  $\epsilon_{c2}$ . This table also shows the ratio of the two values  $R(\epsilon_{c2})_{exp/Rich}$ , and these ratios are plotted in Fig. 4(d). In seven of the eight cases, the experimentally observed longitudinal strain was greater than the predicted value. Table 3 and Fig. 4(d) show that, in general, Eq. (2) provides a reasonable to conservative estimate of the axial strain at the peak compressive stress in the confined core.

### PROPOSED DESIGN PROCEDURE

In the proposed design procedure, spiral reinforcement design is based upon a useable stress instead of the nominal yield stress of the spiral reinforcement. The proposed design procedure provides a means to calculate the useable strain in the spiral reinforcement, which in turn is used to determine the useable stress from the stress-strain curve of the particular spiral wire.

Step 1 in the procedure determines the level of confined compressive strength  $f_{c2,dsgn}$  required for the core concrete in the compression member at  $\Delta_2$ . Using an approach consistent with the ACI 318 Code and AASHTO Design Specification, this core strength enables the member to carry the same axial load after the loss of the concrete cover that it carried prior to concrete cover failure

$$f_{c2,dsgn} = \frac{f_{co}(A_g - A_{st})}{A_{core}} \quad (13)$$

Step 2 calculates the confining pressure  $f_{2-2,dsgn}$ , which is required for the core concrete to reach its desired strength. From Eq. (1),  $f_{2-2,dsgn}$  is calculated as

$$f_{c2,dsgn} = \frac{1}{4.1}(f_{2-2,dsgn} - f_{co}) \quad (14)$$

Step 3 determines the longitudinal strain  $\epsilon_{c2,dsgn}$  at  $\Delta_2$ . This strain is estimated from Eq. (15), which is taken from Eq. (2)

$$\epsilon_{c2,dsgn} = \epsilon_{co} \left( 5 \frac{f_{c2,dsgn}}{f_{co}} - 4 \right) \quad (15)$$

Step 4 determines the transverse strain in the concrete core  $\epsilon_{ct2,dsgn}$ , which occurs at  $\Delta_2$ . The value of  $\epsilon_{ct2,dsgn}$  is calculated as

$$\epsilon_{ct2,dsgn} = 0.41\epsilon_{c2,dsgn} - 0.105\epsilon_{co} \quad (16)$$

The development of Eq. (16) is discussed more fully as follows.

In Step 5, from strain compatibility, the useable strain in the spiral reinforcement  $\epsilon_{sp2,dsgn}$  is the same as the transverse strain in the concrete core  $\epsilon_{ct2,dsgn}$ . This relationship applies at all strains, including those at  $\Delta_2$ . This relationship is expressed as

$$\epsilon_{sp2,dsgn} = \epsilon_{ct2,dsgn} \quad (17)$$

Thus, the value of useable strain is determined by the compression member geometry and concrete material properties. The useable strain is not dependent upon the stress-strain curve of the particular spiral wire that is used. The chosen spiral wire must possess sufficient ductility to achieve this strain value.

Step 6 in the procedure determines the useable stress  $f_{sp2,dsgn}$  from the useable strain  $\epsilon_{sp2,dsgn}$  and the stress strain curve for the particular spiral wire under consideration. Thus, while the useable strain is independent of the stress-strain curve of the spiral, the useable stress does depend upon the stress-strain curve. The ideal situation is to utilize the stress-strain curve of the spiral in its in-place, or spiraled, state. It is more likely, however, that only a stress-strain curve from a tension test of an unspiraled wire will be available, which may not accurately represent the behavior of the spiraled wire. In this case, the value obtained may need to be modified to ensure a proper design. This is discussed more fully in References 3 to 6.

Step 7 determines the required volumetric ratio of spiral reinforcement from Eq. (18), which is a rearranged form of Eq. (5)

$$\rho_{sp,dsgn} = \frac{2f_{c2,dsgn}}{f_{sp2,dsgn}} \quad (18)$$

Finally, Step 8 computes the required pitch  $s_{dsgn}$  from Eq. (19), which is a rearranged form of Eq. (4)

$$s_{dsgn} = \frac{4A_{sp}}{d_{sp}\rho_{sp,dsgn}} \quad (19)$$

### Tangent dilation ratio relationship

A key component of the proposed design procedure is Eq. (16), which describes the relationship between transverse strain and longitudinal strain of the concrete core. This relationship is referred to as the tangent dilation ratio relationship.

Figure 5(a) shows an idealized plot of transverse strain (or spiral strain) versus longitudinal strain for a compression member. The tangent dilation ratio  $\eta_{tan}$  is defined as the

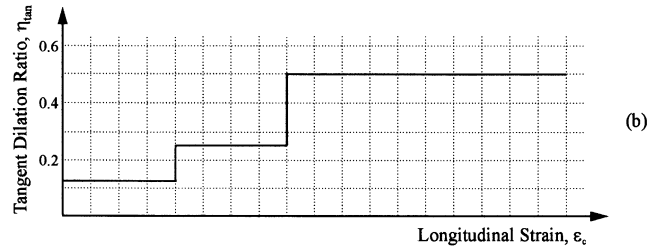
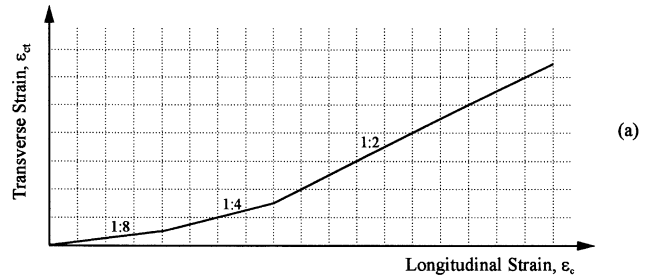


Fig. 5—Tangent dilation ratio: (a) idealized plot of transverse strain versus longitudinal strain; and (b) corresponding tangent dilation ratio.

slope of the curve of transverse strain versus longitudinal strain at any point along the curve

$$\eta_{tan} = \frac{d\epsilon_{ct}}{d\epsilon_c} \quad (20)$$

Figure 5(b) is a plot of  $\eta_{tan}$  versus longitudinal strain for the idealized plot of transverse strain shown in Fig. 5(a). Equation (20) is rearranged and integrated to calculate  $\epsilon_{ct}$ , the transverse strain in the concrete at any longitudinal strain

$$\epsilon_{ct} = \int_{\epsilon_c=0}^{\epsilon_c} \eta_{tan} d\epsilon_c \quad (21)$$

If the integration is performed up to an axial strain  $\epsilon_{c2}$  corresponding to  $\Delta_2$ , the area under the curve, denoted  $A_{\eta_{tan2}}$ , is equal to  $\epsilon_{ct2}$

$$\epsilon_{ct2} = \int_{\epsilon_c=0}^{\epsilon_{c2}} \eta_{tan} d\epsilon_c = A_{\eta_{tan2}} \quad (22)$$

Graybeal and Pessiki compared the experimentally determined values of transverse strain at  $\Delta_2$ , measured with strain gages on the spiral reinforcement, with the values of transverse strain obtained using the experimentally determined tangent dilation ratios. In every case, the value of transverse strain at  $\Delta_2$  measured with strain gages was within 12% of the value of strain computed as the area under the plot of transverse strain versus longitudinal strain. Details are given in References 3 and 4.

Figure 5(a) and (b) are idealizations to illustrate the concept of a tangent dilation ratio. Figure 6(a) shows the tangent dilation ratio relationship proposed by Graybeal and Pessiki to describe the spirally confined compression members

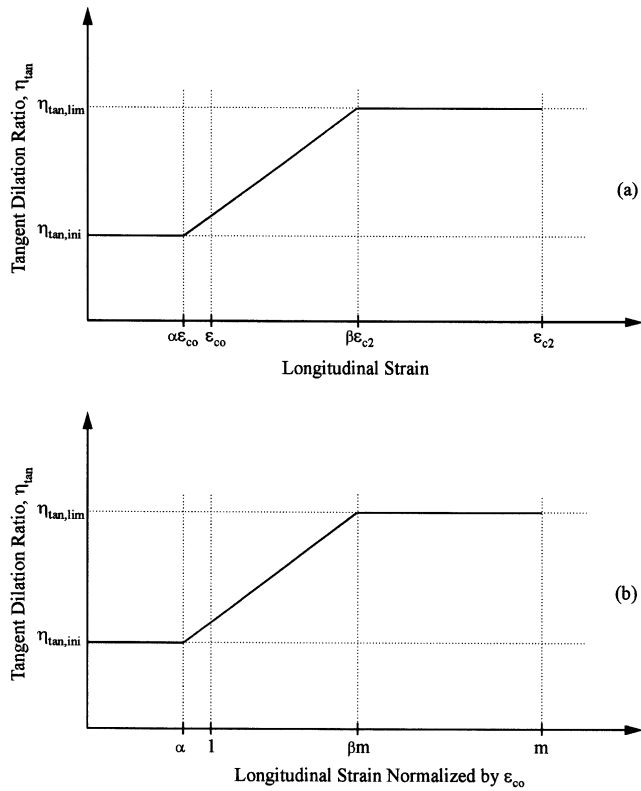


Fig. 6—Proposed tangent dilation relationship: (a) basic relationship; and (b) normalized by  $\epsilon_{co}$ .

between  $\epsilon_c = 0$  and  $\epsilon_{c2}$ . This figure shows that the tangent dilation ratio has an initial constant value  $\eta_{tan,ini}$  up to a longitudinal strain of  $\alpha\epsilon_{co}$ . At this point, the tangent dilation ratio increases in a linear manner to a second constant value of  $\eta_{tan,lim}$ . This limiting value is reached at a longitudinal strain of  $\beta\epsilon_{c2}$ .

Figure 6(b) shows the same plot with the longitudinal strain normalized by the unconfined concrete strain  $\epsilon_{co}$ . Accordingly, the parameter  $m$  is defined as

$$m = \frac{\epsilon_{c2}}{\epsilon_{co}} \quad (23)$$

As was shown in Eq. (22), the area under the tangent dilation ratio curve between  $\epsilon_c = 0$  and  $\epsilon_{c2}$ , denoted as  $A_{\eta_{tan2}}$ , is equivalent to  $\epsilon_{ct2}$ . Calculating the area shown in Fig. 6(a) provides the area  $A_{\eta_{tan2}}$  as follows

$$A_{\eta_{tan2}} = \epsilon_{co} \left( \frac{1}{2} \alpha (\eta_{tan,ini} - \eta_{tan,lim}) + m \left( \frac{1}{2} \eta_{tan,ini} \beta - \frac{1}{2} + \eta_{tan,lim} \beta + \eta_{tan,lim} \right) \right) \quad (24)$$

The following values are proposed for the variables  $\alpha$ ,  $\beta$ ,  $\eta_{tan,ini}$ , and  $\eta_{tan,lim}$ :  $\alpha = 0.7$ ;  $\beta = 0.6$ ;  $\eta_{tan,ini} = 0.2$ ; and  $\eta_{tan,lim} = 0.5$ . Inserting these proposed values into Eq. (24) leads to

$$A_{\eta_{tan2}} = \epsilon_{co} (m(0.41) - 0.105) \quad (25)$$

Again, noting that  $A_{\eta_{tan2}}$  equals  $\epsilon_{ct2}$ , this equation can be written as Eq. (16) presented previously.

## SERIES 2 TESTS

The Series 2 tests were performed to evaluate the proposed design procedure. The Series 2 tests included six 356 mm (14 in.) diameter compression member specimens made with six different spiral wires. Complete details of the Series 2 tests are given in References 5 and 6.

### Experiment details

The Series 2 tests are also described in Table 1. Specimen details, instrumentation, fabrication procedures, and loading procedures for the Series 2 tests were similar to the Series 1 tests. Each specimen was designed using an unconfined concrete compressive strength of 55.2 MPa (8.0 ksi). The nominal yield stress of the spiral reinforcement varied from 538 to 1345 MPa (78 to 195 ksi), and the useable stress varied from 545 to 1131 MPa (79 to 164 ksi).

Wires A' through D' were the same wires A through D treated in the Series 1 tests. Spiral wire E' had a nominal diameter of 9.1 mm (0.36 in.) and a reported yield stress of 1345 MPa (195 ksi). Finally, spiral wire F' had a nominal diameter of 10.9 mm (0.43 in.) diameter and a reported yield stress of 1276 MPa (185 ksi). Spiral wires E' and F' were not perfectly circular in cross section, but instead had small reductions in section formed by grooves in the wires along their lengths.

Based on material testing, the unconfined concrete compressive strength  $f_{co}$  for the Series 2 tests was taken as 52.1 MPa (7.55 ksi), and the axial concrete strain corresponding to the unconfined concrete strength  $\epsilon_{co}$  was taken as 0.0027.

The six different spiral reinforcement wires treated in this research were supplied by three different manufacturers. The results of tension tests of wires E' and F' are included in Fig. 2 and Table 2. It is noted that the curves for wires E' and F' were obtained from straight tension specimens that had never been turned into a spiral.

Due to a fabrication error, Specimen 14-B' failed prematurely during testing in the heavily confined region at the top of the specimen. The results from this specimen are excluded from the remaining discussions.

### Summary of spiral design

The proposed design procedure was used to design the spiral for each specimen. Design parameters for the Series 2 specimens included a member diameter of 356 mm (14 in.), a cover distance of 51 mm (2 in.), and concrete compressive strength  $f_{co}$  equal to 55.2 MPa (8.0 ksi). The calculation of useable strain proceeded as follows. First,  $f_{c2,dsgn}$  was calculated from Eq. (13) to be 109 MPa (15.8 ksi). From Eq. (14), the confining pressure  $f_{2-2,dsgn}$  was calculated as 13.0 MPa (1.88 ksi). Next,  $\epsilon_{c2,dsgn}$  was calculated by Eq. (15) as 0.0158, and  $\epsilon_{ct2,dsgn}$  was calculated from Eq. (16) to be 0.0062. Finally, Eq. (17) was used to obtain a value for  $\epsilon_{sp2,dsgn}$  equal to 0.0062. This was the useable strain value used in the design of the specimens. The useable stresses were determined for each wire at that strain, and Eq. (18) and (19) were used to calculate  $\rho_{sp,dsgn}$  and finally the spiral pitch  $s_{dsgn}$ .

**Table 4—Summary of results of Series 2 tests**

Series 1																
Design				Experiment							Richart, Brandzaeg, and Brown	Ratios				
Identifi- cation	$\epsilon_{c2,dsgn}$	$\epsilon_{sp2,dsgn}$	$f_{sp2,dsgn}$ , MPa	$\Delta f_{c12,dsgn}$ , MPa	$\epsilon_{sp2,exp}$	$f_{sp2,exp}$ , MPa	$P_2$ , MN	$f_{c2,exp}$ , MPa	$\Delta f_{c12,exp}$ , MPa	$\epsilon_{c2,exp}$	$\Delta f_{c12,Rich}$ , MPa	$R(\epsilon_{c2})_{exp}$ /dsgn	$R(\epsilon_{sp2})_{exp}$ /dsgn	$R(f_{sp2})_{ex}$ p/dsgn	$R(\Delta f_{c12})_{ex}$ p/dsgn	$R(\Delta f_{c12})_{ex}$ p/Rich
14-A'	0.0158	0.0062	545	53.2	0.0063	545	5.54	105.4	53.4	0.0153	53.2	0.97	1.02	1.00	1.00	1.00
14-C'	0.0158	0.0062	745	53.1	0.0063	752	5.56	105.9	53.8	0.0219	53.6	1.39	1.02	1.01	1.01	1.00
14-D'	0.0158	0.0062	758	53.2	0.0091	917	5.91	112.8	60.7	0.0344	64.3	2.18	1.47	1.21	1.14	0.95
14-E'	0.0158	0.0062	1131	53.1	0.0122	1338	4.97	94.1	42.1	0.0231	62.8	1.46	1.97	1.18	0.79	0.67
14-F'	0.0158	0.0062	1110	53.2	0.0086	1310	5.03	95.4	43.3	0.0206	62.8	1.30	1.39	1.18	0.81	0.69

Note: 1 kip = 0.00445 MN; 1 ksi = 6.895 MPa; and 1 in. = 25.4 mm.

**Axial load behavior**

The axial load-axial shortening response of each Series 2 specimen is shown in Fig. 3(c). Similar to the Series 1 tests, each specimen exhibited the idealized behavior illustrated in Fig. 1. Key results from the Series 2 tests are presented in Table 4.

**Longitudinal strains**

Table 4 shows the experimentally obtained values and design values of  $\epsilon_{c2}$  and the ratio of these two values  $R(\epsilon_{c2})_{exp/dsgn}$ . As was done with the Series 1 tests, the experimental value  $\epsilon_{c2,exp}$  was obtained as the average measured strain in the longitudinal reinforcement at  $\Delta_2$ . The  $R(\epsilon_{c2})_{exp/dsgn}$  ratios are plotted versus the design useable spiral stress in Fig. 7(a). Table 4 and Fig. 7(a) show that the experimental values exceeded the design values in every case except Specimen 14-A', where the value of  $R(\epsilon_{c2})_{exp/dsgn}$  was 0.97. This indicates that the proposed design procedure gives a reasonable to conservative prediction of longitudinal strain at  $\Delta_2$ .

**Spiral strains and stresses**

Table 4 shows the experimentally obtained and design values of  $\epsilon_{sp2}$  and the ratio of these two values  $R(\epsilon_{sp2})_{exp/dsgn}$ . These ratios are plotted versus the design useable spiral stress in Fig. 7(b). Table 4 and Fig. 7(b) show that, in all cases, the measured strains were equal to or greater than the design values. Table 4 and Fig. 7(c) show similar results for the experimental and design values of  $f_{sp2}$ . From the aforementioned results, it is clear that the proposed design method provides a reasonable to conservative estimate of the values of the spiral strains and stresses, and thus a reasonable to conservative estimate of the confining pressure provided by the spiral reinforcement.

**Confined concrete strength**

An experimental value for the increase in compressive strength of the confined concrete core  $\Delta f_{c12,exp}$  was computed using the same procedure described previously in Eq. (9) and (10). This experimental value is compared with the design value  $\Delta f_{c12,dsgn}$  in Table 4 and Fig. 7(d), which show the ratio of these values  $R(\Delta f_{c12})_{exp/dsgn}$  plotted versus the design value of useable stress in the spiral reinforcement. Table 4 and Fig. 7(d) show that Specimens 14-A', 14-C', and 14-D' either achieved or exceeded the design values of core strength enhancement based on the spiral design useable stress. For these specimens,  $R(\Delta f_{c12})_{exp/dsgn}$  ranged from 1.00 to 1.14. In contrast, the core strength enhancement in Specimens 14-E' and 14-F' fell approximately 20% below the design values.

Table 4 also shows the Richart, Brandzaeg, and Brown-predicted values of  $\Delta f_{c12,Rich}$  and  $R(\Delta f_{c12})_{exp/Rich}$ , which is the ratio of  $\Delta f_{c12,exp}$  to  $\Delta f_{c12,Rich}$ . This ratio is also plotted versus the design value of useable stress in the spiral reinforcement for each specimen in Fig. 7(e). Table 4 and Fig. 7(e) show that Specimens 14-A' and 14-C' satisfied the Richart, Brandzaeg, and Brown prediction of increased compressive strength of the concrete core. Specimen 14-D' nearly satisfied the prediction, falling short by only 5%. Specimens 14-E' and 14-F', however, achieved only 67 and 69% of the Richart, Brandzaeg, and Brown predictions. These results show that Specimens 14-A', 14-C', and 14-D' exhibited experimental core strength increases consistent with the stresses observed in the spiral steel, but Specimens 14-E' and 14-F' did not. This suggests that the Richart, Brandzaeg, and Brown equation may have a limit on its range of applicability for higher strength steels.

**DISCUSSION**

The Series 2 results showed that specimens designed with useable stresses that ranged from 545 to 758 MPa (79 to 110 ksi) achieved their design strengths, and that the specimens designed with useable stresses of 1131 and 1110 MPa (164 and 161 ksi) did not achieve their design strengths. Therefore, based upon the results of this research, it is concluded that the proposed design procedure provides satisfactory spiral designs for spiral steels with useable stress values up to 758 MPa (110 ksi). As discussed as follows, this conclusion is applicable to the 356 mm (14 in.) diameter compression members, and is also thought to be applicable to the 610 mm (24 in.) diameter compression members.

Three key relationships used in the design procedure were demonstrated to provide acceptable results for design purposes for spiral steels with useable stress values up to 110 ksi (758 MPa). First, Eq. (15) (taken from Richart, Brandzaeg, and Brown Eq. (2)) provides reasonable to conservative estimates of longitudinal strain at  $\Delta_2$ . Second, Eq. (16), the tangent dilation ratio relationship proposed by Graybeal and Pessiki, provides reasonable to conservative estimates of strains in the spiral reinforcement at  $\Delta_2$ . The result of these first two relationships is that the proposed design procedure provides conservative estimates of the strains and stresses in the spiral reinforcement at  $\Delta_2$ , and thus conservative estimates of the confining stress on the core concrete at  $\Delta_2$ . Finally, Eq. (14) (taken from Richart, Brandzaeg, and Brown Eq. (1)), which relates confining pressure to axial strength enhancement, was found to be valid for the specimens made with useable stress values up to 110 ksi (758 MPa).

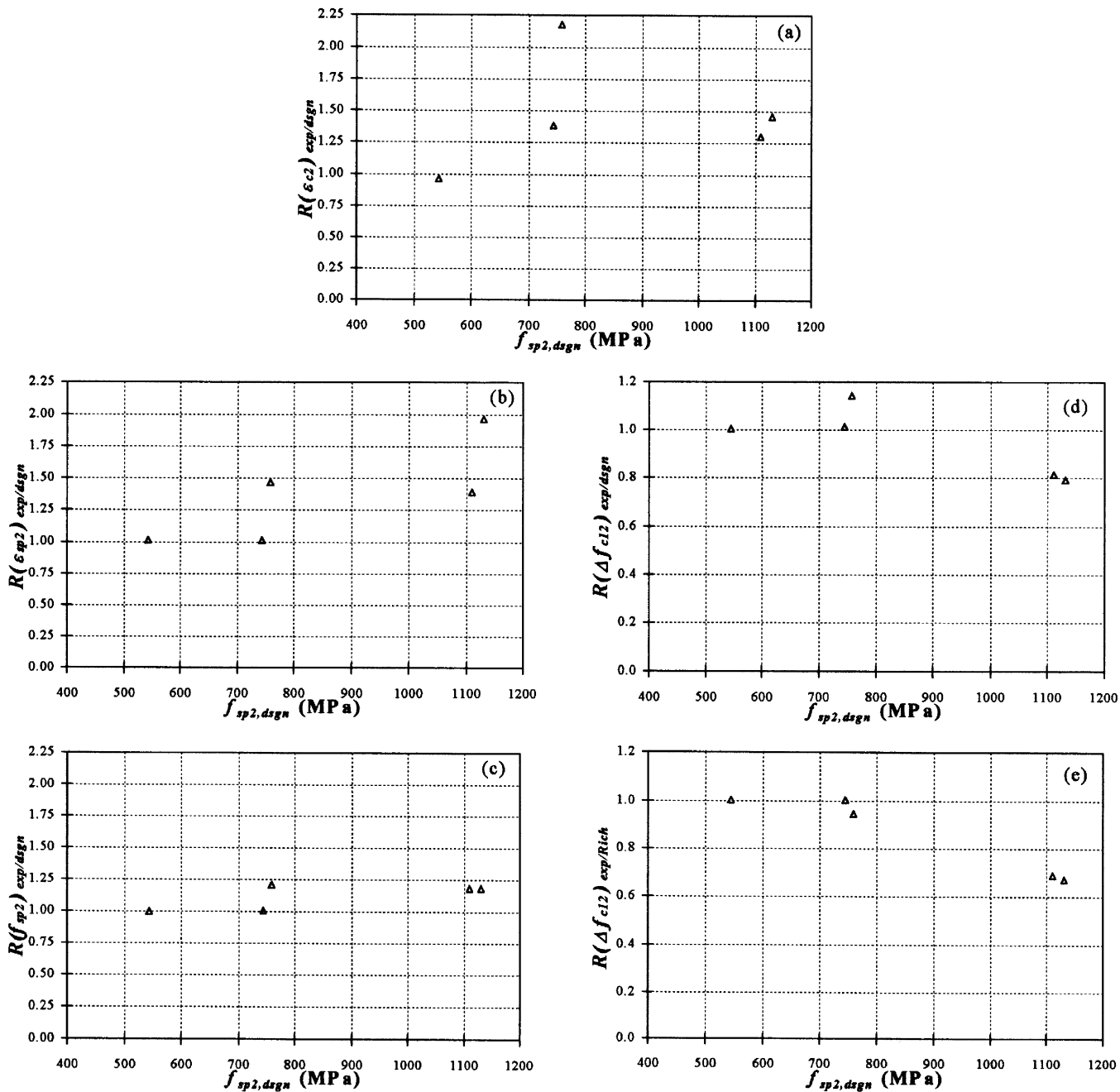


Fig. 7—Series 2 results: (a)  $R(e_{c2})_{exp/dsgn}$  versus  $f_{sp2,dsgn}$ ; (b)  $R(e_{sp2})_{exp/dsgn}$  versus  $f_{sp2,dsgn}$ ; (c)  $R(f_{sp2})_{exp/dsgn}$  versus  $f_{sp2,dsgn}$ ; (d)  $R(\Delta f_{c12})_{exp/dsgn}$  versus  $f_{sp2,dsgn}$ ; and  $R(\Delta f_{c12})_{exp/Rich}$  versus  $f_{sp2,dsgn}$ .

Even though the longitudinal strains, spiral strains, and spiral stresses were all adequately predicted using the proposed design procedure, Specimens 14-E' and 14-F' failed to reach their design strengths. Thus, there is a limit to the range applicability of the proposed design procedure. Several factors, discussed as follows, may contribute to the finding that Specimens 14-E' and 14-F' failed to reach their design strengths.

#### In-place stress-strain curve of spiral reinforcement

The designs of Specimens 14-A' through 14-D' were based upon useable stresses determined from stress-strain curves from tension tests on straightened segments of spiral wires. For Specimens 14-E' and 14-F', the design was based on useable

stresses obtained from the stress-strain curves from unspiraled wires. As noted previously, the process of turning a steel wire into a spiral introduces residual stresses within the cross section of the wire, which changes its tension stress-strain behavior. Analyses reported elsewhere<sup>3-6</sup> showed significant rounding or softening of the stress-strain curves at strain values near where the useable stress values were extracted. Thus, for Specimens 14-E' and 14-F', the actual useable stress values were likely overestimated, and, as a consequence, the specimens may have been underdesigned. Analyses presented in References 5 and 6 show that the useable stress value were overestimated by approximately 15% when basing the useable stress values on curves from tests on unspiraled wires as opposed to wires in their in-place spiraled state.

## Variable confining stress provided by spiral reinforcement

The Richart, Brandzaeg, and Brown prediction of the confined strength of the core concrete (Eq. (1)) is based in large part on tests of compression members with relatively low strength (mild steel) spiral reinforcement and on tests of cylinders where a constant lateral pressure was applied using a pressurized fluid. In both instances, the confining pressure is approximately constant (for a mild steel, the lateral confining stress is constant once the spiral yields).

A different situation occurs where confinement is provided by high-strength spiral reinforcement. In this later case, the confining pressure continues to increase with increased spiral strain well beyond the strains at which a mild steel bar would have yielded. The confining stress does not become constant until yielding occurs. Equation (1), developed for the case of essentially constant confinement, may not be applicable for the confinement histories of Specimens 14-E' and 14-F'.

## Stiffness of spiral reinforcement

Specimens 14-E' and 14-F' had the highest useable stress values of the Series 2 specimens. Because the spirals for all Series 2 specimens were designed to provide the same confining pressure, Specimens 14-E' and 14-F' had a smaller volumetric ratio of spiral steel as compared with the remainder of the specimens. As a result, these specimens also had smaller spiral stiffnesses (where stiffness is computed as spiral area multiplied by elastic modulus, per unit height along the member) as compared with the remainder of the specimens. The stiffness of the spiral influences the confining stress developed at any spiral strain. The stiffness of the spiral may influence the rate at which the core expands with axial strain, and thus the rate at which confining stress develops with axial strain.

It is noted that Eq. (1) adequately predicted the behavior of the 610 mm (24 in.) diameter Series 1 specimens. Redesign of these specimens would result in an increase in the volumetric ratio of spiral reinforcement, and thus an increase in the stiffness of the spiral reinforcement for these specimens. Thus, Eq. (1) would be expected to also be applicable for these redesigned specimens.

## CONCLUSIONS

The conclusions of this research are as follows:

1. The proposed design procedure provides satisfactory spiral designs for spiral steels with useable stress values up to 758 MPa (110 ksi). This conclusion is applicable to the specimen geometries (including the 610 mm (24 in.) diameter Series 1 specimens) and material strengths treated in this research;

2. From the previous conclusion, it follows that current design requirements that limit the design yield stress of spiral reinforcement in compression members to 414 MPa (60 ksi) may be modified to permit higher stresses. Spiral steel stresses in excess of 414 MPa (60 ksi) can be used to design spiral reinforcement in compression members similar to the specimens treated in this research; and

3. Three key relationships used in the proposed design procedure provide acceptable results for the design purposes. First, Eq. (15) (Eq. (2) from Richart, Brandzaeg, and Brown) provides reasonable to conservative estimates of the longitudinal strain at  $\Delta_2$ . Second, Eq. (16), the tangent dilation ratio relationship proposed by Graybeal and Pessiki, provides reasonable to conservative estimates of transverse strains in the

concrete, and thus, strains in the spiral reinforcement at  $\Delta_2$ . Third, Eq. (14) (Eq. (1) from Richart, Brandzaeg, and Brown), which relates confining pressure to axial strength enhancement, is valid for compression members made with useable stress values up to 758 MPa (110 ksi).

## FUTURE RESEARCH

Additional research is needed to fully explain the behavior of Specimens 14-E' and 14-F', where the observed increases in core strength were below the strength increases that were expected based on the level of lateral confining pressure that was developed. This future work should focus on the role of residual stresses on the stress-strain properties of the spiral reinforcement and on the role of spiral stiffness and variable confining pressures throughout the response of a compression member on the resulting strength enhancement of the concrete core.

## ACKNOWLEDGMENTS

This research was funded by the Precast/Prestressed Concrete Institute, through a Daniel P. Jenny Fellowship, and by the Center for Advanced Technology for Large Structural Systems at Lehigh University. Additional support was provided by Concrete Technology Corp., Sumiden Wire Products Corp., Florida Wire and Cable, Inc., and Neturen Co., Ltd. Support from the sponsors is gratefully acknowledged. The findings and conclusions presented in this report are those of the authors, and do not necessarily reflect the views of the sponsors.

## CONVERSION FACTORS

1 in.	=	25.4 mm
1 ksi	=	6.895 MPa
1 kip	=	0.00445 MN

## NOTATION

$A_{core}$	=	core concrete area measured to outside diameter of spiral
$A_g$	=	gross area of compression member
$A_{st}$	=	total area of longitudinal reinforcement
$A_{sp}$	=	total cross-sectional area of spiral wires
$A_{\eta_{tan2}}$	=	area under tangent dilation ratio curve between $\epsilon_c = 0$ and $\epsilon_{c2}$
$d_c$	=	compression member diameter
$d_{sp}$	=	diameter of spiral measured to outside of wire
$d_{sw}$	=	diameter of individual spiral wire
$f_{2-2}$	=	lateral confining stress at $\Delta_2$
$f_{2-2,dsgn}$	=	design value of lateral confining stress at $\Delta_2$
$f_{co}$	=	compressive strength of unconfined concrete
$f_{c2}$	=	compressive strength of confined concrete at $\Delta_2$
$f_{c2,dsgn}$	=	design value of confined concrete compressive strength
$f_{c2,exp}$	=	experimental value of stress in core at $\Delta_2$
$f_{sp}$	=	stress in spiral reinforcement
$f_{sp2}$	=	stress in spiral reinforcement at $\Delta_2$
$f_{sp2,dsgn}$	=	design value of useable stress in spiral
$f_{sp2,exp}$	=	experimental value of stress in spiral at $\Delta_2$
$f_{sy}$	=	yield stress of spiral reinforcement
$f_{sy,nom}$	=	nominal yield stress of spiral reinforcement as reported by spiral
$f_y$	=	yield stress of longitudinal reinforcement
$m$	=	$\epsilon_{c2}$ normalized by $\epsilon_{co}$
$n_{sp}$	=	number of spiral wires bundled to form single turn of spiral
$P_o$	=	nominal compression member capacity
$P_1$	=	load on compression member just prior to cover spalling
$P_2$	=	load on compression member at confined peak after cover spalling
$P_{failure}$	=	load on compression member at failure
$P_s$	=	force in longitudinal reinforcement
$R(f_{sp2,exp}/f_{sy,nom})$	=	ratio of $f_{sp2,exp}$ to $f_{sy,nom}$
$R(\Delta f_{c12,exp}/dsgn)$	=	ratio of $\Delta f_{c12,exp}$ to $\Delta f_{c12,dsgn}$
$R(\Delta f_{c12,exp}/Rich)$	=	ratio of $\Delta f_{c12,exp}$ to $\Delta f_{c12,Rich}$
$R(\epsilon_{c2,exp}/dsgn)$	=	ratio of $\epsilon_{c2,exp}$ to $\epsilon_{c2,dsgn}$

$R(\epsilon_{c2})_{exp/Rich}$	= ratio of $\epsilon_{c2,exp}$ to $\epsilon_{c2,Rich}$
$R(\epsilon_{sp2})_{exp/dsg}$	= ratio of $\epsilon_{sp2,exp}$ to $\epsilon_{sp2,dsgn}$
$s$	= spiral pitch
$s_{dsgn}$	= design value of spiral pitch
$\alpha$	= percentage of $\epsilon_{co}$ at which tangent dilation ratio begins to increase
$\beta$	= percentage of $\epsilon_{c2}$ at which tangent dilation ratio becomes constant
$\epsilon_{c2}$	= axial strain in concrete corresponding to $f_{c2}$
$\epsilon_{c2,dsgn}$	= design value of longitudinal strain at $\Delta_2$
$\epsilon_{c2,exp}$	= experimental value of longitudinal strain at $\Delta_2$
$\epsilon_{c2,Rich}$	= longitudinal strain at $\Delta_2$ estimated using Richart, Brandzaeg, and Brown
$\epsilon_{co}$	= axial strain in concrete corresponding to $f_{co}$
$\epsilon_{ct}$	= transverse concrete strain
$\epsilon_{ct2}$	= transverse concrete strain at $\Delta_2$
$\epsilon_{ct2,dsgn}$	= design value of transverse concrete strain at $\Delta_2$
$\epsilon_{sp2,dsgn}$	= design value of strain in spiral reinforcement at $\Delta_2$
$\epsilon_{sp2,exp}$	= experimental value of strain in spiral reinforcement at $\Delta_2$
$\epsilon_{su}$	= ultimate strain in spiral reinforcement
$\Delta_1$	= compression member axial shortening corresponding to $P_1$
$\Delta_2$	= compression member axial shortening corresponding to $P_2$
$\Delta f_{c12,exp}$	= experimental value of increase in strength of concrete core
$\Delta f_{c12,dsgn}$	= design value of increase in strength of concrete core
$\Delta f_{c12,Rich}$	= increase in strength of concrete core predicted using Richart, Brandzaeg, and Brown
$\Delta f_{failure}$	= compression member axial shortening corresponding to $P_{failure}$
$\eta_{tan}$	= tangent dilation ratio
$\eta_{tan,ini}$	= proposed initial tangent dilation ratio
$\eta_{tan,lim}$	= proposed limiting tangent dilation ratio
$\rho_l$	= area ratio of longitudinal reinforcement

$\rho_{sp}$	= volumetric ratio of spiral reinforcement
$\rho_{sp,dsgn}$	= design value of volumetric ratio of spiral reinforcement

## REFERENCES

1. ACI Committee 318, "Building Code Requirements for Structural Concrete (ACI 318-95) and Commentary (318R-95)," American Concrete Institute, Farmington Hills, Mich., 1995, 369 pp.
2. AASHTO, "AASHTO LRFD Bridge Design Specifications," American Association of State Highway and Transportation Officials, First Edition, Washington, D.C., 1994.
3. Graybeal, B. A., "Confinement Effectiveness of High-Strength Spiral Reinforcement in Prestressed Concrete Piles," MS thesis, Department of Civil and Environmental Engineering, Lehigh University, Bethlehem, Pa., 1998, 228 pp.
4. Graybeal, B. A., and Pessiki, S. P., "Confinement Effectiveness of High-Strength Spiral Reinforcement in Prestressed Concrete Piles," Report No. 98-01, Center for Advanced Technology for Large Structural Systems, Apr. 1998, 164 pp.
5. Mudlock, M., "Design of High-Strength Spiral Reinforcement for Prestressed Concrete Piles," MS thesis, Department of Civil and Environmental Engineering, Lehigh University, Bethlehem, Pa., 1999, 185 pp.
6. Mudlock, M., and Pessiki, S., "Design of High-Strength Spiral Reinforcement for Prestressed Concrete Piles," Report No. 99-12, Center for Advanced Technology for Large Structural Systems, Lehigh University, July 1999, 134 pp.
7. Considère, A., "Résistance à la compression du béton armé et du béton fretté," *Génie Civil*, 1903.
8. Richart, F. E.; Brandzaeg, A.; and Brown, R. L., "A Study of the Failure of Concrete under Combined Compressive Stresses," *University of Illinois Bulletin*, V. XXVI, No. 12, Nov. 20, 1928, 104 pp.
9. Richart, F. E.; Brandzaeg, A.; and Brown, R. L., "The Failure of Plain and Spirally Reinforced Concrete in Compression," *University of Illinois Bulletin*, V. XXVI, No. 31, Apr. 2, 1929, 74 pp.
10. Richart, F. E., and Brown, R. L., "An Investigation of Reinforced Concrete Columns," *University of Illinois Bulletin*, V. XXVI, No. 40, June 5, 1934, 94 pp.